

# Search for $\text{Sc}_3\text{XB}$ ( $X=\text{In, Tl, Ga, Al}$ ) perovskites superconductors and proximity of weak ferromagnetism

B. Wiendlocha, J. Tobola,\* and S. Kaprzyk

Faculty of Physics and Applied Computer Science, AGH University of Science and Technology, Aleja. Mickiewicza 30, 30-059 Krakow, Poland

(Received 25 July 2005; revised manuscript received 13 February 2006; published 28 April 2006)

A possibility for an additional family of intermetallic perovskite superconductors  $\text{Sc}_3\text{XB}$ , with  $X=\text{Tl, In, Ga, and Al}$ , is presented as a result of Korringa-Kohn-Rostoker (KKR) electronic structure and pseudopotential phonon calculations. The large values of computed McMillan-Hopfield parameters on scandium suggest the appearance of superconductivity in  $\text{Sc}_3\text{XB}$  compounds. On the other hand, the possibility of weak itinerant ferromagnetic behavior of  $\text{Sc}_3\text{X}$  systems is indicated by the small magnetic moment on Sc atoms in the two cases of  $X=\text{Tl}$  and  $\text{In}$ . In addition, the electronic structure and resulting superconducting parameters for the realistic case of boron-deficient systems  $\text{Sc}_3\text{XB}_x$  are computed, using KKR method with the coherent potential approximation, by replacing boron atom with a vacancy. The comparison of the calculated McMillan-Hopfield parameters of the  $\text{Sc}_3\text{XB}$  series with corresponding values in related  $\text{MgCNi}_3$  and  $\text{YRh}_3\text{B}$  superconductors is also shown, finding favorable trends for superconductivity.

DOI: [10.1103/PhysRevB.73.134522](https://doi.org/10.1103/PhysRevB.73.134522)

PACS number(s): 74.10.+v, 74.25.Jb, 74.25.Kc, 74.62.Dh

## I. INTRODUCTION

The motivation to search for a superconductivity in the intermetallic series of  $\text{Sc}_3\text{XB}$  compounds was inspired by very interesting and nontypical superconductivity of  $\text{MgCNi}_3$  perovskite,<sup>1</sup> with the critical temperature  $T_c \approx 8$  K. First of all, the large amount of nickel atoms would suggest ferromagnetic properties in this compound, and indeed, a propensity to form a magnetic state is really large, due to the van Hove singularity near the Fermi level.<sup>2</sup> This may be a reason for some of the unexpected effects, that were observed experimentally in this material<sup>3–6,70</sup> despite  $\text{MgCNi}_3$  belonging to the electron-phonon type superconductors<sup>7,8</sup> with a high isotope effect on carbon.<sup>9</sup>

Among other intermetallic perovskites similar to  $\text{MgCNi}_3$ , only one compound,  $\text{YRh}_3\text{B}$ , was earlier reported to be a superconductor, with  $T_c=0.76$  K.<sup>10</sup> However, since the superconductivity in  $\text{MgCNi}_3$  has been discovered, no other superconductor has been found so far. Systematic experimental study<sup>11</sup> showed some indications of superconductivity in  $\text{CaB}_x\text{Pd}_3$  ( $T_c \approx 1$  K) and  $\text{NbB}_x\text{Rh}_3$  ( $T_c \approx 6$  K), but the superconducting phase was finally not identified. In addition, no evidence of superconductivity was found experimentally in  $\text{ZnCNi}_3$ ,<sup>12</sup> despite the calculated electronic structure being very close to that of  $\text{MgCNi}_3$ . Here, the carbon deficiency was proposed as a possible explanation.<sup>13</sup>

The predictions of superconductivity in  $\text{Sc}_3\text{InB}$  were announced in our conference paper.<sup>14</sup> Interesting properties of  $\text{Sc}_3\text{InB}$  encouraged us to investigate electronic structure and electron-phonon coupling (EPC) along the whole isoelectronic series of  $\text{Sc}_3\text{XB}$  compounds, with  $X=\text{Tl, In, Ga, Al}$ , and detailed results of our theoretical study are presented in this work.

The crystal structure of  $\text{Sc}_3\text{XB}$  (space group  $Pm-3m$ ,  $\text{CaTiO}_3$  type) is shown in Fig. 1. The synthesis of Tl- and In-containing cubic perovskites was reported,<sup>15</sup> while Ga- and Al-containing compounds were hypothetical. The perov-

skite structure of  $\text{Sc}_3\text{XB}$  may also be viewed as a  $\text{Cu}_3\text{Au}$ -type cubic  $\text{Sc}_3\text{X}$ , with additional boron atom placed in the center (see Fig. 1). In particular, the  $\text{Sc}_3\text{In}$  system was found to exist, in two polymorphic forms:<sup>16</sup> one is the above-mentioned, not well known cubic  $\text{Cu}_3\text{Au}$ , detected under a high pressure,<sup>17</sup> and the second one is hexagonal  $\text{Ni}_3\text{Sn}$ -type, in which weak ferromagnetism was observed.<sup>18</sup> Ferromagnetism of the hexagonal  $\text{Sc}_3\text{In}$  guided us to study possibility of magnetic behaviors in the binary series of cubic  $\text{Sc}_3\text{X}$  compounds. Indeed, the computations showed that the cubic  $\text{Sc}_3\text{In}$  is magnetic as well as the hexagonal phase. For other systems, the results of electronic structure calculations are also presented, although we are not aware of the existence of these compounds. Noteworthy, spin-polarized computations of  $\text{Sc}_3\text{XB}$  converged to the nonmagnetic ground state. We

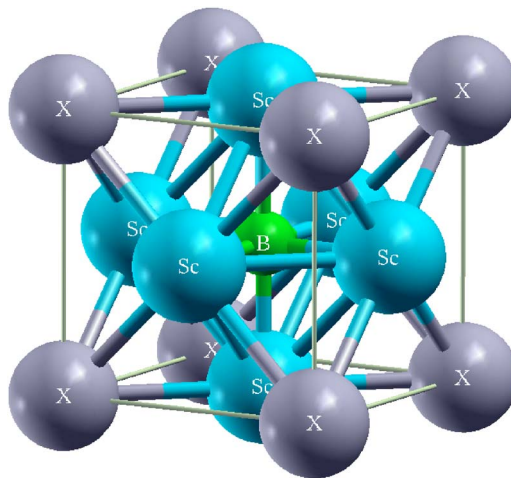


FIG. 1. (Color online) Crystal structure of the  $\text{Sc}_3\text{XB}$  perovskite. The atomic positions are: X: 1a (0,0,0), B: 1b (1/2, 1/2, 1/2), and Sc: 3c (0, 1/2, 1/2), (1/2, 0, 1/2), (1/2, 1/2, 0). If the central B atom is removed, perovskite structure changes into  $\text{Cu}_3\text{Au}$ -type one.

also intend to underline some correlations between tendency to superconductivity in  $\text{Sc}_3\text{XB}$  on one hand, and to weak ferromagnetism in the corresponding  $\text{Sc}_3\text{X}$ , on the other hand.

## II. CALCULATIONS

First-principle calculations of the superconducting parameters, due to the subtle nature of such phenomenon, are still challenging problem in the density functional theory computations. McMillan<sup>19</sup> in his fundamental work showed, that the electron-phonon coupling calculations might be decoupled into electronic and phonon contributions, when several approximations were used. The commonly used formula for the essential parameter for superconductivity, resulting from generalization of his concept to multiatomic compounds, is as follows:

$$\lambda = \sum_i \frac{\eta_i}{M_i \langle \omega_i^2 \rangle} = \sum_i \lambda_i, \quad (1)$$

where  $\lambda$  is the EPC constant and  $i$  corresponds to all atoms in the unit cell, with  $\eta_i$  being the electronic, and  $M_i \langle \omega_i^2 \rangle$  lattice contribution to the electron-phonon interaction parameter.

The electronic part of the EPC constant–McMillan-Hopfield parameters  $\eta_i$ ,<sup>19,20</sup> which describe the response of electrons from Fermi surface to displacements of atoms, are computed within the Gaspari-Györfy<sup>21</sup> method, using the so-called rigid-muffin-tin approximation (RMTA). The relevant formula for  $\eta$  is<sup>22</sup> ( $i$  subscript is dropped)

$$\eta = \sum_l \frac{(2l+2)n_l(E_F)n_{l+1}(E_F)}{(2l+1)(2l+3)n(E_F)} \times \left| \int_0^{R_{MT}} r^2 R_l(r) \frac{dV(r)}{dr} R_{l+1}(r) dr \right|^2, \quad (2)$$

where  $V(r)$  is the self-consistent, spherically symmetric potential on given atom site,  $R_{MT}$  is the radius of the  $i$ th muffin-tin (MT) sphere,  $R_l(r)$  is a regular solution of the radial Schrödinger equation (normalized to unity inside the MT sphere), and  $n_l(E_F)$  is the  $l$ th partial density of states at the Fermi level ( $E_F$ ) on the considered site.

This method usually involves three main assumptions:<sup>23</sup>

(i) *Rigid-ion approximation*, in which potential inside the MT sphere moves rigidly with the ion, and the change in crystal potential, caused by the atom displacement, is given by the potential gradient.

(ii) *Local-vibration approximation*, in which the off-diagonal terms in the EPC constant are neglected (i.e.,  $\lambda_{ij} = \delta_{ij}\lambda_i$ ). More generally  $\lambda = \sum_{ij} \lambda_{ij}$ , where  $(i, j)$  refer to two atoms in the unit cell.

(iii) *Spherical band approximation*, which leads to only dipole transitions ( $l \rightarrow l+1$ ) in Eq. (2).

It is known that all mentioned assumptions give satisfactory results for the transition metal elements and cubic-site symmetry. In simple metals, assumptions (i) and (ii) generally underestimate<sup>24</sup> EPC, due to a poorly screened crystal potential, whereas the corrections to (iii) are expected to be small for cubic transition metals.<sup>25</sup>

In order to allow for independent calculations of the electron and phonon subsystems, another simplification is necessary. Estimation of  $\langle \omega_i^2 \rangle$  in Eq. (1), using exclusively phonon density of states  $F(\omega)$  instead of full electron-phonon coupling function  $\alpha^2 F(\omega)$ , requires an assumption that the electron-phonon interaction is independent of phonon frequency  $\omega$ . Thus, the electron-phonon interaction factor  $\alpha^2(\omega)$  cancels<sup>71</sup> when calculating  $\langle \omega_i^2 \rangle$  (see, e.g., Ref. 26).

The assumption that EPC magnitude does not change with phonon frequency, is well fulfilled, e.g., in niobium,<sup>27</sup> but may not exhibit the same behavior in multiatom compounds. However, the RMTA method was successfully used for analyzing EPC in many superconducting materials, such as pure metals,<sup>28</sup> binary alloys,<sup>29</sup> A-15 compounds,<sup>30</sup> transition metal carbides,<sup>31,32</sup> borocarbides,<sup>33</sup> or metal-hydrogen system.<sup>34</sup> Reasonable results (as far as  $\lambda$  is concerned) were usually obtained, even in such an unusual superconductor, as  $\text{MgB}_2$ .<sup>35</sup> This formalism was also helpful in discussing phonon-based effects in high-temperature superconductors.<sup>23,36</sup> Certainly, in order to better understand the electron-phonon interactions in a superconductor, one has to perform more elaborated calculations, using the Eliashberg gap equations (see, for example, results for  $\text{MgB}_2$ ).<sup>37,38</sup> Nevertheless, such separate electronic structure and phonon calculations, together with the simplified RMTA framework, are very useful and efficient tools at early stage when searching for new superconducting systems.

Following this methodology, McMillan-Hopfield parameters and phonon frequency moments were calculated for  $\text{Sc}_3\text{XB}$  compounds, and then, using Eq. (1) EPC parameters  $\lambda$  were deduced.

Electronic structure calculations were performed using the Korringa-Kohn-Rostoker (KKR) method, which in the case of disordered systems (Sec. II B) was implemented together with the coherent potential approximation (CPA), as described in detail in Ref. 39. Additionally, for ordered compounds, computations were performed with the full-potential (FP) code, based on the FP-KKR formalism, widely discussed by many authors,<sup>40</sup> with technical details shown, e.g., when applying to Si,<sup>41</sup> or to the electric field gradient calculations.<sup>42</sup> In our practice, extracting bands was done with a quasilinear algorithm<sup>43</sup> that allows for more precise and less time-consuming band structure calculations, compared to conventional techniques. The crystal potential was constructed within the local density approximation (LDA), applying the Perdew-Wang<sup>44</sup> formula for the exchange-correlation part. For all calculations angular momentum cut-off  $l_{max}=3$  was set. Highly converged results were obtained for about 120  $\mathbf{k}$ -point grid in the irreducible part of Brillouin zone (IRBZ), but they were also checked for convergence using more dense  $\mathbf{k}$ -mesh and  $l_{max}=4$ . Electronic densities of states were computed using the tetrahedron  $\mathbf{k}$ -space integration technique (up to 700 tetrahedrons in IRBZ). In the case of investigated compounds, the differences between the full potential and spherical potential KKR calculations of the density of states (DOS) values at the Fermi level were of order of a few percentage points. The justification for using different kinds of approximations, when computing McMillan-Hopfield parameters, was supported by checking

the numerical values on changing different input data (such as nonrelativistic versus semirelativistic calculations, type of exchange-correlation potential, radii of MT spheres), which we also found to differ on the range of a few percentage. Such accuracy we consider satisfactory to explain trends in the number of systems, but for more detailed analysis, the fine computations with the full potential will be necessary, especially if the Fermi surface specific features become important.

Phonon calculations were undertaken for realistic approximation of the phonon part of the electron-phonon coupling constant  $\lambda$ , i.e.,  $\langle\omega_i^2\rangle$  parameter in Eq. (1). We used the PWSCF package,<sup>45</sup> where the plane-wave pseudopotential technique and perturbation theory<sup>46</sup> were implemented. For Sc, B, and Tl atoms, ultrasoft pseudopotentials were employed, and for Al, Ga, and In, norm-conserving pseudopotentials were used. LDA parametrization of Perdew and Zunger<sup>47</sup> was implemented. Plane-wave kinetic energy and charge density cutoffs were set to 30 and 350 Ry, respectively. The Brillouin zone special points integration technique of Methfessel and Paxton<sup>48</sup> (with smearing parameter  $\sigma=0.02$  Ry) was used during the calculations. In order to obtain the phonon DOS  $F(\omega)$ , first the dynamical matrices on (5,5,5)  $\mathbf{q}$ -point grid were calculated. Using the Fourier transformation on the same grid, real-space interatomic force constants were then computed. The final phonon densities of states were calculated from the dynamical matrices calculated by Fourier interpolation of the force constant to (10,10,10)  $\mathbf{q}$ -point grid and using the tetrahedron integration method. The combined results of the KKR electronic structure study and the phonon DOS calculations were then used to estimate the EPC constant.

We also estimated the superconducting transition temperature  $T_c$  from McMillan formula<sup>19</sup> in Eq. (3), using the modified factor  $\langle\omega\rangle/1.2$ .<sup>49,50</sup>

$$T_c = \frac{\langle\omega\rangle}{1.2} \exp\left[-\frac{1.04(1+\lambda)}{\lambda - \mu^*(1+0.62\lambda)}\right]. \quad (3)$$

The absolute value of  $T_c$  depends also on Coulomb pseudopotential parameter  $\mu^*$ , and its influence on value of  $T_c$  is additionally discussed.

### A. Predictions of superconductivity in $\text{Sc}_3\text{XB}$

Crystal structure and atomic positions of the  $\text{Sc}_3\text{XB}$  system are presented in Fig. 1. For all investigated, ordered  $\text{Sc}_3\text{XB}$  compounds, lattice constants were calculated from total energy minimum, as a first step of the PWSCF phonon calculations. Both KKR electronic structure and phonon computations were then performed with these equilibrium lattice parameters. Except for  $X=\text{Al}$ , semirelativistic calculations results are presented here. In order to obtain the McMillan-Hopfield parameters, the following MT spheres radii (in the lattice constant  $a_0$  unit) were employed:  $R_{\text{Sc}}=0.325$ ,  $R_X=0.360$ , and  $R_{\text{B}}=0.174$ . Equation (2) suggests that  $\eta_i$  parameter may be sensitive to a choice of  $R_{\text{MT}}$ , so we also checked the influence of the computational geometry on final results. The  $R_{\text{MT}}$  spheres variation in the range of 15% changed the results about 5%. The difference in obtained

TABLE I. Lattice parameters in  $\text{Sc}_3\text{XB}$  series in atomic units (1 Bohr=0.5292 Å).

Compound	$a$ experimental <sup>a</sup>	$a_0$ calculated
$\text{Sc}_3\text{TlB}$	8.541	8.650
$\text{Sc}_3\text{InB}$	8.618	8.610
$\text{Sc}_3\text{GaB}$	—	8.550
$\text{Sc}_3\text{AlB}$	—	8.610

<sup>a</sup>See Ref. 15.

results, for somewhat arbitrary MT geometry, may be treated as the computational accuracy of the  $\eta_i$  value.

In Table I, results of lattice constant optimization for  $\text{Sc}_3\text{XB}$  are summarized. In both existing compounds, the agreement between experimental and theoretical values is quite good. The variation of  $a_0$  with atom  $X$  reflects the change in ionic radius of the  $X$ -element, from the smallest one for Ga to the largest one for Tl. For  $\text{Sc}_3\text{TlB}$  calculated value  $a_0$  is larger than the experimental one, which is not so common a case. Noteworthy, a similar effect was also observed in  $\text{YRh}_3\text{B}$ .<sup>51,52</sup> The smaller experimental value of  $a$  in  $\text{Sc}_3\text{TlB}$  could indicate that the measured sample was boron deficient, as it was earlier suggested for  $\text{YRh}_3\text{B}$ .<sup>52</sup>

Figure 2 presents electronic DOS in the  $\text{Sc}_3\text{XB}$  compounds. As we can see, the DOS shape is very similar along this series, due to the same number of valence electrons. Noteworthy, even  $\text{Sc}_3\text{AlB}$ , where Al contains only  $s$ - and  $p$ -like orbitals, exhibits electronic structure quite similar to other  $\text{Sc}_3\text{XB}$  compounds, with closed  $nd^{10}$  shell on the  $X$  atom. This shell forms a semicore level, located about 1 Ry below  $E_F$ . It supports the widely accepted conclusion that  $3d$  Ga,  $4d$  In and  $5d$  Tl electrons build up core-like levels, and the effect on upper-lying electronic states (particularly near  $E_F$ ) is small.

The most important part of the density of states near the Fermi level in all compounds is formed from Sc  $d$ -states, hybridized with  $p$ -states from B and X. The site contributions to  $n(E_F)$  are presented in Table II.<sup>72</sup> Electronic dispersion curves for the representative compound,  $\text{Sc}_3\text{InB}$ , are shown in Fig. 3, and they are very similar in other cases. The DOS sharp peak, located just below  $E_F$ , comes from a flat band, which is clearly seen in  $E(\mathbf{k})$  along the  $X$ - $M$ - $\Gamma$  direction. Generally, the bands in  $\text{Sc}_3\text{InB}$  are more dispersive, comparing, e.g., to  $\text{MgCNi}_3$ ,<sup>53,54</sup> or  $\text{Sc}_3\text{In}$  (see Fig. 13). Two separated, lowest-lying bands ( $E < -0.3$  Ry) are formed from  $s$ -states of  $X$  and B atoms, with notably large contribution from Sc.

The most interesting feature of electronic structure, suggesting superconductivity appearance, is related to large McMillan-Hopfield parameters, seen along the whole  $\text{Sc}_3\text{X}$  series (see Table II). In scandium, typically for transition element,  $d$ - $f$  scattering channel gives the most important contribution to  $\eta_i$ . For boron and  $X$ -element, only the  $p$ - $d$  channel contributes to  $\eta_i$ . Note that, although the  $\eta_{\text{B}}$  values were found to be the largest in our systems,  $\eta_{\text{Sc}}$  occurred to be more important in calculation of  $\lambda$ , since it is counted three times (3 Sc atoms in unit cell), and has lower value of  $M_i\langle\omega_i^2\rangle$  (see Table II). Despite a noticeable density of states

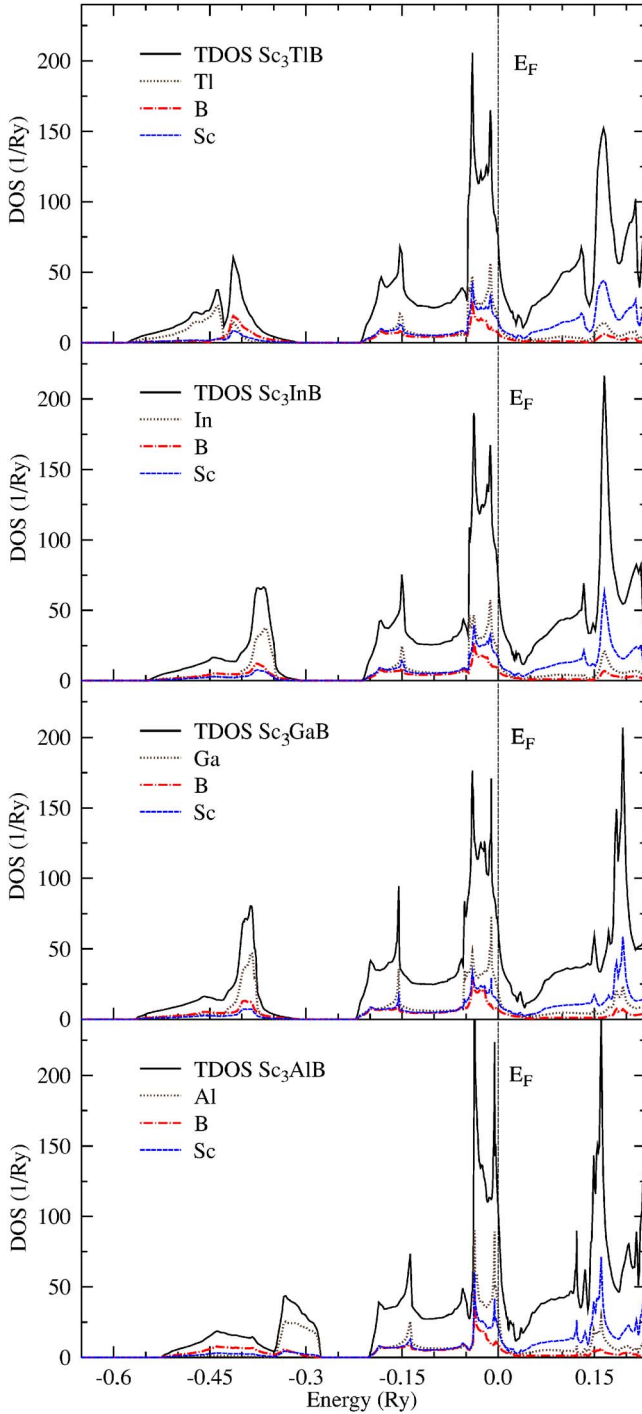


FIG. 2. (Color online) KKR total DOS of isoelectronic  $\text{Sc}_3\text{XB}$  perovskites, calculated at equilibrium lattice constants  $a_0$ . Site-decomposed densities for X, B, Sc, are plotted in brown (dotted line), red (dash-dotted line), and blue (dashed line), respectively. The Fermi level is shifted to zero and marked by a vertical line.

at the Fermi level,  $\eta_X$  has negligible value. The accuracy of computed  $\eta_i$ , associated with different MT geometry, is about 1 mRy/Bohr<sup>2</sup> for scandium and 2 mRy/Bohr<sup>2</sup> for boron.

The phonon DOS and its evolution with the X-element is given in Fig. 4. The most striking feature of the presented  $F(\omega)$  is the “rigid-band-like” modification with the mass

TABLE II. Site-decomposed electronic and phonon properties of  $\text{Sc}_3\text{XB}$ .  $n(E_F)$  is given in 1/Ry,  $\eta_i$  in mRy/Bohr<sup>2</sup>,  $\omega_i$  in THz, and  $M_i\langle\omega_i^2\rangle$  in mRy/Bohr<sup>2</sup>.

Atom	$n(E_F)$	$\eta_i$	$\sqrt{\langle\omega_i^2\rangle}$	$M_i\langle\omega_i^2\rangle$	$\lambda_i$
Sc	20.0	18	3.7	50	0.36
Tl	17.4	2	3.7	226	0.01
B	7.6	32	15.0	204	0.16
Sc	20.0	19	4.5	76	0.25
In	16.3	1	4.5	193	0.01
B	6.7	34	14.1	181	0.19
Sc	19.0	18	4.6	80	0.23
Ga	18.4	2	4.6	124	0.01
B	6.5	35	14.7	197	0.18
Sc	21.6	18	5.2	100	0.18
Al	21.5	1	5.2	60	0.02
B	6.4	30	14.2	183	0.16

variation of the X-element (note, that the mass distribution in the unit cell markedly changes). The highest peak in Fig. 4 marks the weakly dispersive part of acoustic branches, associated with the X-atom vibrations. As one can see, as the mass of X decreases, the range of acoustic modes broadens, which is manifested in a shift of their flat parts towards higher frequencies; i.e., the peak moves from 2 THz ( $X=\text{Tl}$ ) to 6 THz ( $X=\text{Al}$ ). Generally, the phonon spectrum consists of two separate areas: the high-frequency part includes essentially phonon modes of light B, with frequencies above 12 THz, and the lower-frequency part, below 12 THz, contains mainly X and Sc states. This behavior was also characteristic for the dynamic properties of  $\text{MgCNi}_3$

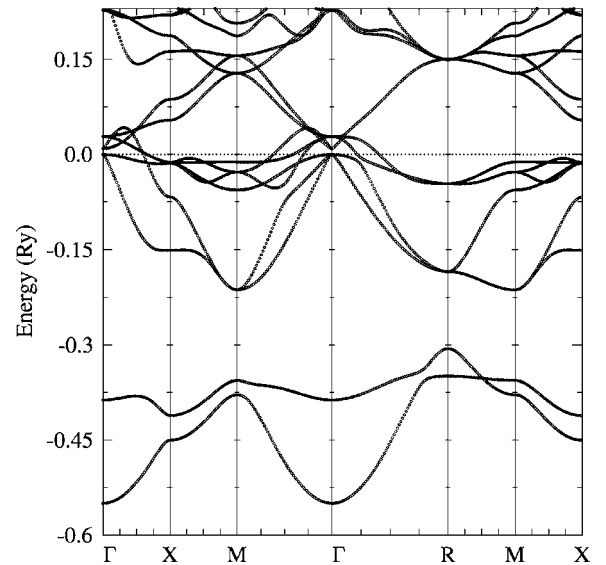


FIG. 3. Electronic dispersion curves  $E(\mathbf{k})$  along high-symmetry directions in  $\text{Sc}_3\text{InB}$  perovskite, calculated at equilibrium lattice constant  $a_0$ . The Fermi level is shifted to zero and marked by a horizontal line.

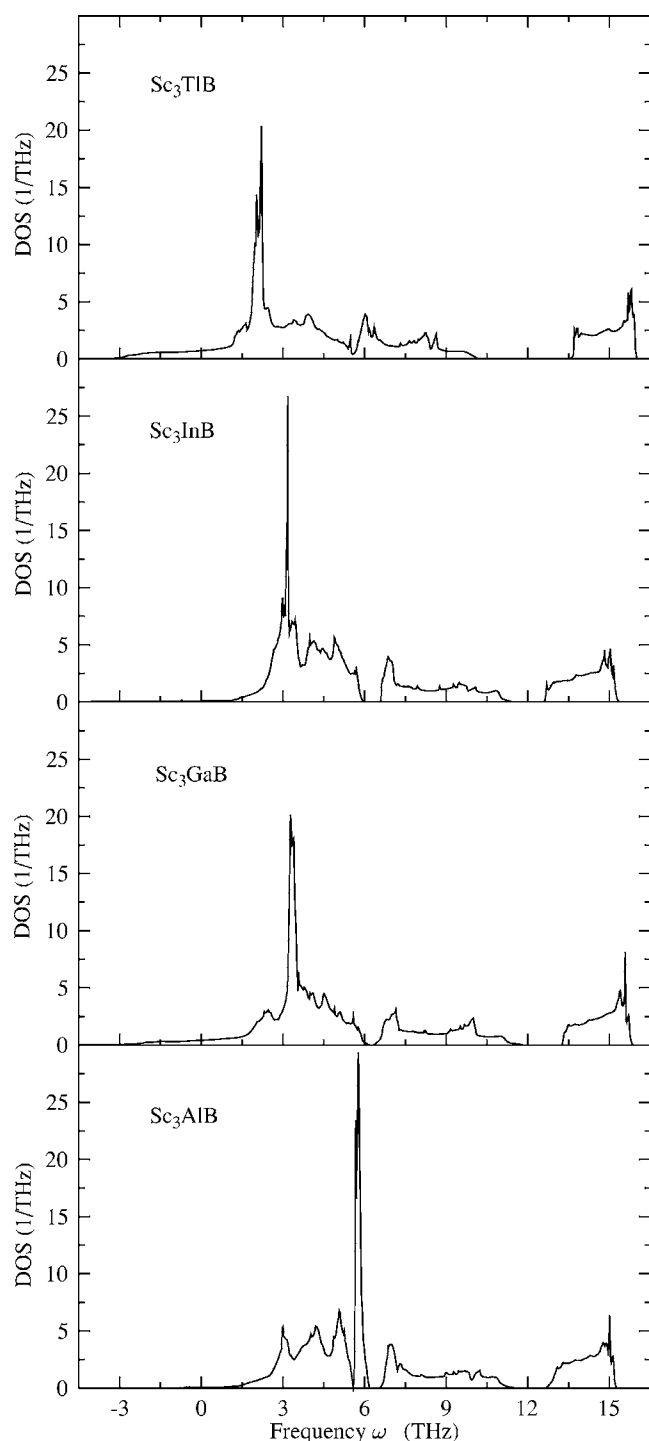


FIG. 4. Phonon DOS  $F(\omega)$  in  $\text{Sc}_3\text{XB}$  perovskites, calculated at equilibrium lattice constants  $a_0$ .

compound, where carbon vibrations had the highest frequencies.<sup>55</sup>

Let us remark that in the phonon calculations for all compounds, we met some problems with imaginary frequencies appearing near the BZ center ( $\Gamma$ ), and additionally for  $X=\text{Tl}$  and  $\text{Ga}$ , near the  $R$  point (in Fig. 4 they are visible as negative frequency tails). These eigenvalues correspond to three optical modes, and at  $\Gamma$  and  $R$  points only Sc atoms vibrate in these modes, with eigenvectors lying in three

planes perpendicular to the Sc-B bonds. Physically, the occurrence of imaginary frequencies may indicate either the instability of the perfect perovskite structure (favoring crystal distortion) or non-negligible anharmonic contributions.

Similarly, unstable phonon branches were detected in  $\text{MgCNi}_3$ ,<sup>55,56</sup> occurring at different high-symmetry points ( $X, M$ ). These branches corresponded mainly to anharmonic Ni vibrations, resulted from a double-well potential,<sup>55-57</sup> in which Ni was placed. However, due to the shallowness of the double well, no stable long-range structural distortion was found there, and the perovskite structure was stabilized dynamically. The origin of unstable vibrations in  $\text{Sc}_3\text{XB}$  is attractive problem itself, but more detailed analysis of their dynamical properties is beyond the scope of this paper.

In summary, the influence of the negative frequency range on phonon density of states is not so critical (the related energy bands are strongly dispersive). This should not affect much the  $\langle \omega_i^2 \rangle$  calculations. The total weight of the negative-frequency area is about 0.5% in  $\text{Sc}_3\text{InB}$  and  $\text{Sc}_3\text{AlB}$ , 2.5% in  $\text{Sc}_3\text{GaB}$ , and 5% in  $\text{Sc}_3\text{TlB}$ . Thus, in the case of  $X=\text{In}$  and  $\text{Al}$ , the “negative tail” was negligible in the frequency moments calculations. For two remaining compounds ( $X=\text{Ga}$  and  $\text{Tl}$ ) the tail was cut off at about 0.5 THz and  $F(\omega)$  was extrapolated to reach  $\omega=0$  in Debye-like manner. Because the phonon DOS obtained for  $\text{Sc}_3\text{TlB}$  seems less reliable, in this case the evaluation of the superconducting parameters should be treated rather qualitatively.

Having the phonon DOS, we may proceed to estimate the EPC strength. The mean phonon frequencies for constituent atoms were computed from the phonon DOS, using the above mentioned analysis of the spectrum:  $\langle \omega_i^2 \rangle$  for  $X$  and Sc were calculated from the lower-frequency part of the spectrum, and were assumed to be the same for both atoms. As expected, the lowest value of  $\langle \omega_i^2 \rangle$  is observed in the thallium compound. The average  $\langle \omega_B^2 \rangle$  were computed from the high-frequency part of DOS, and resulted in significantly larger values, due to a small mass of boron (see Table II). Note that taking the same value of  $\langle \omega_i^2 \rangle$  for all atoms might be incorrect,<sup>31</sup> and disagrees with the atomic-like character of  $\eta_i$  ( $M_i \omega_i^2$  corresponds to an effective force constant, so it is also a site-dependent quantity). In systems where atoms have markedly different masses, the lightest element would be favored in that way, as is shown below. Therefore, the phonon DOS was divided into high- and low-frequency parts in the  $\langle \omega_i^2 \rangle$  calculations.

The values of total EPC constant  $\lambda$ , i.e., sum over atomic contributions, shown in Table II, are gathered in Table III together with the critical temperature values. In all investigated compounds the main contribution to  $\lambda$  comes from scandium. Due to the lowest value of  $\langle \omega_{\text{Sc}}^2 \rangle$  parameter,  $\text{Sc}_3\text{TlB}$  has the highest  $\lambda$ . Superconducting transition temperature  $T_c$  was estimated using Eq. (3), with typical value of Coulomb pseudopotential  $\mu^*=0.13$ . As one can notice, all compounds with calculated  $\lambda$  in the range of 0.7–1.2, and  $T_c \approx 10$  K are medium-, or even strong-coupling superconductors in the RMTA framework.

To verify the influence of employed  $\mu^*$  on  $T_c$  magnitude, we plotted the value of  $T_c$  versus  $\mu^*$  in the reasonable range of  $0.09 < \mu^* < 0.21$  (see Fig. 5). Transition temperatures de-

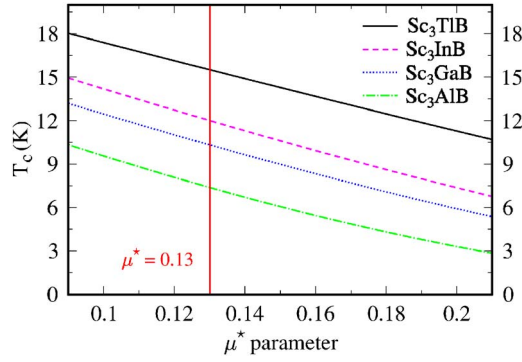


FIG. 5. (Color online) Influence of the  $\mu^*$  parameter on critical temperature  $T_c$ . Vertical line marks  $\mu^*=0.13$ .

crease almost linearly with  $\mu^*$  in this range, and even for a large value of  $\mu^*=0.21$ ,  $T_c$  is still enough high to be detectable in the typical low-temperature measurements.

We also examined how our results changed when  $\langle\omega_i^2\rangle$  was taken to be equal for all atoms. For example, in  $\text{Sc}_3\text{InB}$  we obtained  $\lambda=1.6$  with  $\lambda_B=1.1$  and  $\lambda_{\text{Sc}}=0.17$ , when setting  $\sqrt{\langle\omega^2\rangle}=5.66$  THz, as derived from the entire phonon spectrum. The resulting critical temperature  $T_c=26$  K was much higher than the previous value, and probably much overestimated, due to the overestimation of the boron contribution.

The pressure effect on electronic properties of  $\text{Sc}_3\text{XB}$  was additionally inspected by decreasing lattice parameter in KKR computations (in the range of 0%–5%). The variation of the most important parameters—total density of states at  $E_F$  and McMillan-Hopfield parameters for boron and scandium—is summarized in Table IV. The observed tendency is again similar in the whole series. In spite of the  $n(E_F)$  decrease with volume shrinking,  $\eta_i$  parameters increase with ratio about  $d \ln \eta_B / d \ln V \approx -2$  and  $d \ln \eta_{\text{Sc}} / d \ln V \approx -1.5$ . These results suggest that external pressure may enhance  $T_c$ , as observed in  $\text{MgCNi}_3$ ,<sup>3,4</sup> but the opposite effect of lattice stiffening may be dominant.

To have a better insight into the magnitude of McMillan-Hopfield parameters in  $\text{Sc}_3\text{XB}$ , we performed similar electronic structure calculations for the existing, related perovskite superconductors,  $\text{MgCNi}_3$  and  $\text{YRh}_3\text{B}$ , applying the experimental values of lattice parameters (in Bohr units): 7.205 (Ref. 1) and 7.870 (Ref. 10), respectively. Since the DOS for  $\text{MgCNi}_3$  was recently published by many authors (e.g., Refs. 53 and 54), we present the KKR DOS for the less known  $\text{YRh}_3\text{B}$  in Fig. 6.

As we can observe from Tables II and V, values of  $\eta_i$  for the transition element (Sc, Ni, Rh) are very similar in all cases. It should be noticed, that the 2- $p$  states of the light

TABLE III. Total EPC constant  $\lambda$  and critical temperature  $T_c$  (in K) for  $\mu^*=0.13$ .  $\langle\omega\rangle$  used in Eq. (3) is also given in K.

	$\text{Sc}_3\text{TIB}$	$\text{Sc}_3\text{InB}$	$\text{Sc}_3\text{GaB}$	$\text{Sc}_3\text{AlB}$
$\lambda$	1.25	0.94	0.88	0.72
$\langle\omega\rangle$	182	225	226	263
$T_c$	15	12	10	7.5

TABLE IV. Influence of unit cell volume shrinking on electronic critical parameters.  $dn(E_F)/dV$  is given in  $1/(\text{Ry Bohr}^3)$ .

Compound	$\frac{dn(E_F)}{dV}$	$\frac{d \ln \eta_{\text{Sc}}}{d \ln V}$	$\frac{d \ln \eta_B}{d \ln V}$
$\text{Sc}_3\text{TIB}$	0.41	-1.4	-1.9
$\text{Sc}_3\text{InB}$	0.41	-1.5	-2.0
$\text{Sc}_3\text{GaB}$	0.50	-1.2	-2.3
$\text{Sc}_3\text{AlB}$	0.44	-1.4	-2.6

element (boron) contribute only a little to the states near the Fermi level in  $\text{YRh}_3\text{B}$  (see Fig. 6).<sup>51,52</sup> This is the reason for the very small  $\eta_B$  parameter, compared to  $\eta_C$  in  $\text{MgCNi}_3$  and especially  $\eta_B$  in  $\text{Sc}_3\text{XB}$ . In addition, the large atomic mass of rhodium ( $M \approx 103$ ), compared to scandium ( $M \approx 45$ ) or nickel ( $M \approx 59$ ) may be responsible for the low superconducting critical temperature ( $\sim 1$  K) in this compound. The comparison of McMillan-Hopfield parameters in presented perovskites additionally favors superconductivity in  $\text{Sc}_3\text{XB}$  compounds due to relatively low mass of scandium.

### B. Effect of vacancy on the B-site

When dealing with this family of compounds, one has to face with possible crystallographic imperfections of the  $\text{Sc}_3\text{XB}$  structure. The common problem occurring in the intermetallic perovskite borides (and carbides) is related to not fully occupied boron (carbon) position. Note that various boron or carbon deficiencies were observed in many related perovskites,<sup>11</sup> as well as in  $\text{MgCNi}_3$ . This effect is very important for superconductivity, since in  $\text{MgC}_x\text{Ni}_3$  critical tem-

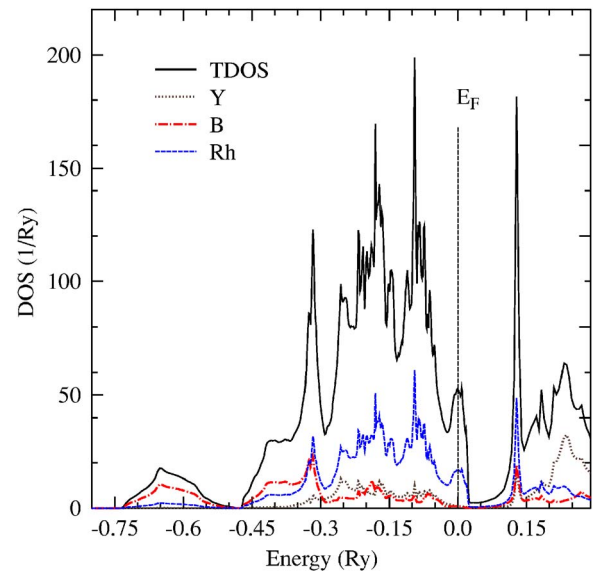


FIG. 6. (Color online) KKR DOS of  $\text{YRh}_3\text{B}$  calculated at experimental lattice parameter. Site-decomposed densities for Y, B, and Rh are plotted in brown (dotted line), red (dash-dotted line), and blue (dashed line), respectively. The Fermi level is shifted to zero and marked by a vertical line.

TABLE V. McMillan-Hopfield parameters (in  $\text{mRy}/\text{Bohr}^2$ ) for  $\text{MgCNi}_3$  and  $\text{YRh}_3\text{B}$ .

Atom	$\eta_i$	Atom	$\eta_i$
Ni	20.4	Rh	17.5
Mg	0.1	Y	1.4
C	9.1	B	1.6

perature decreases linearly with C concentration,<sup>58</sup> and superconductivity disappears for  $x < 0.9$ . The vacancy on the B-site is highly plausible in our compounds, and this effect has to be taken into account in the analysis. This prompted us to perform the calculations of electronic structure and McMillan-Hopfield parameters in  $\text{Sc}_3\text{XB}_x$  from the KKR-CPA method.<sup>39</sup> A vacancy on the boron site was treated as an “empty sphere,” with  $Z=0$  and the same MT radius, as applied for the B atom. In the nonstoichiometric  $\text{Sc}_3\text{XB}_x$  the (1b) position is occupied by B atom and a vacancy with probabilities  $x$  and  $1-x$ , respectively. The electronic structure of such disordered system was calculated using the coherent potential approximation, which allows processing of any finite concentrations, including impurity states.

Site-decomposed DOS at  $E_F$  in  $\text{Sc}_3\text{XB}_x$  [divided by  $n(E_F)$  in stoichiometric  $\text{Sc}_3\text{XB}$ ] and McMillan-Hopfield parameters

versus B concentration, are shown in Fig. 7. At a first glance, one observes that all site contributions to DOS at  $E_F$  decrease in the investigated systems, with decreasing of boron concentration, and reach less than 50% of initial values for  $x=0.85$ . This is unlikely to the rigid-band behavior, where  $E_F$  is expected to move to the left, towards higher DOS (see Fig. 2). More detailed analysis of KKR-CPA DOS in  $\text{Sc}_3\text{XB}_x$  (see also Fig. 12) indicates, that a vacancy on the B site seems to behave as a hole donor, if the pseudogap in DOS, found above  $E_F$ , can be considered as a separation between valence-like and conduction-like bands. Since the potential of the vacancy is much more repulsive, than the potential of B atom, all  $p$ -states (accommodating six electrons) are expelled into higher-energy range (well above  $E_F$ ), against only one electron occupying the  $p$ -shell in the B atom. Consequently, the filling of low-lying conduction-like states decreases, when the vacancy concentration increases.

The analysis of critical parameters for considered vacancy concentrations ( $0.85 < x < 1$ ) shows, that presence of vacancy is very unfavorable for occurrence of superconductivity in these structures, due to a sudden decrease of the most important  $\eta_{\text{Sc}}$  and  $\eta_{\text{B}}$  parameters (see Fig. 7). Using the values of  $\langle \omega_i^2 \rangle$  obtained in the stoichiometric  $\text{Sc}_3\text{XB}$  compounds, the variation of EPC constant and  $T_c$  for boron-deficient structures were analyzed. As we can see in Fig. 8, in

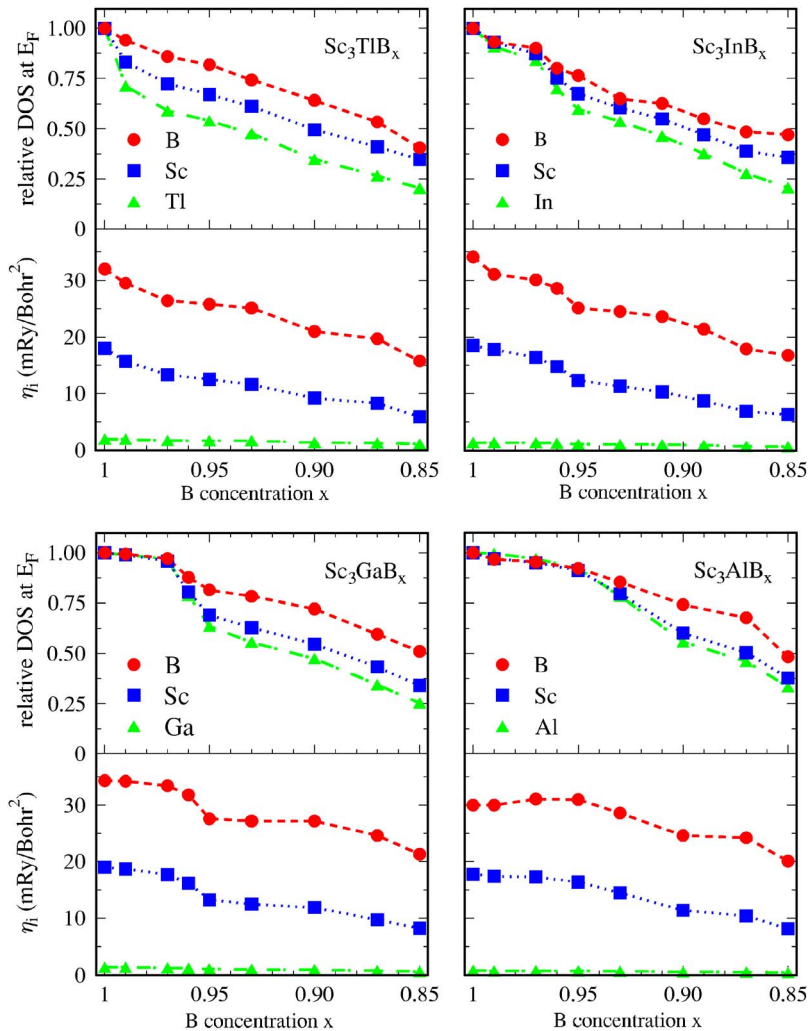


FIG. 7. (Color online) Effect of B-sublattice deficiency in  $\text{Sc}_3\text{XB}_x$  on site-decomposed DOS at the Fermi level (upper panels) and corresponding McMillan-Hopfield parameters (lower panels) computed from KKR-CPA method (see text). In both panels, the corresponding values for B (in red), Sc (in blue), and X (in green) are marked by circles, squares, and triangles, respectively. Lines connecting calculated points are added as a guide to the eye.

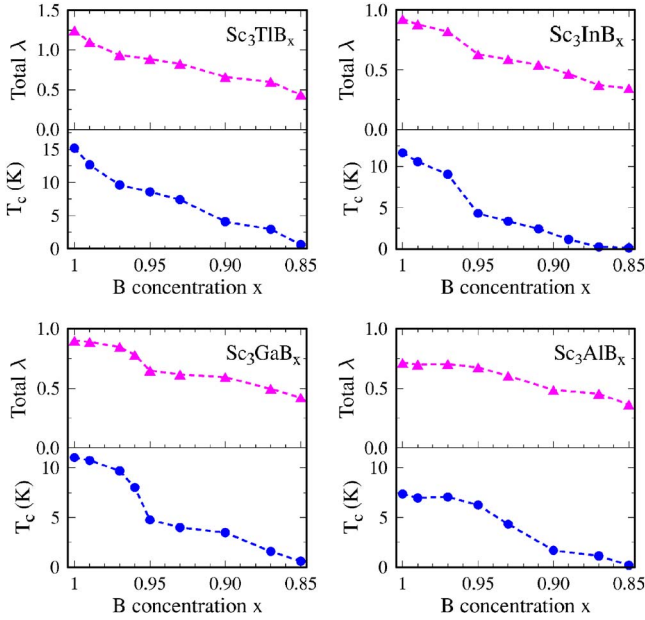


FIG. 8. (Color online) Effect of B-sublattice deficiency in  $\text{Sc}_3\text{XB}_x$  on EPC constant  $\lambda$  (upper panels) and corresponding critical temperature (lower panels). Lines connecting calculated points are added as a guide to the eye.

all systems, the decrease in  $\lambda$  is so fast that superconductivity is practically quenched ( $T_c \sim 0.1$  K) when vacancy concentration reaches 15% (i.e.,  $\text{Sc}_3\text{XB}_{0.85}$ ). Thus, the boron atom occurs to play crucial role in superconductivity onset in  $\text{Sc}_3\text{XB}$ , since even a small boron deficiency may cause a rapid decrease of the critical temperature.

This behavior seems to be similar to  $\text{MgCNi}_3$  case, where lowering of  $T_c$  with an increase of the vacancy concentration on the carbon site was observed experimentally.<sup>58,59</sup> Quite recently, two important investigations were carried out for this system. It was deduced from the specific-heat measurements<sup>60</sup> that in a carbon-deficient sample, low-energy nickel phonon modes (which are probably the most important in superconductivity) were shifted to higher energies. Furthermore, electronic structure calculations performed for  $\text{MgC}_x\text{Ni}_3$  in the range  $0.80 < x < 1$  exhibited the decrease of  $n(E_F)$  with the increasing  $x$ ,<sup>61</sup> but less drastic than in our  $\text{Sc}_3\text{XB}_x$  systems. Disappearance of superconductivity in  $\text{MgC}_x\text{Ni}_3$  seems to result from two unfavorable effects, lowering the DOS at Fermi level combined with increasing phonon frequencies. Taking into account the possibility of similar behavior of low-energy phonon modes in  $\text{Sc}_3\text{XB}_x$  we may suggest that superconductivity in  $\text{Sc}_3\text{XB}$  could be even more sensitive to nonstoichiometry, than in  $\text{MgCNi}_3$ .

### C. Magnetic properties of cubic $\text{Sc}_3\text{X}$

The motivation to study relations between superconductivity in  $\text{Sc}_3\text{XB}$  and magnetism in  $\text{Sc}_3\text{X}$  compounds was inspired by the widely studied weak itinerant ferromagnetism of the hexagonal  $\text{Sc}_3\text{In}$ .<sup>18</sup> In spite of recent interest in this field, the research of the cubic form of  $\text{Sc}_3\text{In}$  has not been carried out so far. To have a possibility of wider comparison

TABLE VI. Lattice parameters in the  $\text{Sc}_3\text{X}$  series in atomic units.

Compound	$a$ experimental <sup>a</sup>	$a_0$ calculated
$\text{Sc}_3\text{Tl}$	—	8.300
$\text{Sc}_3\text{In}$	8.427	8.150
$\text{Sc}_3\text{Ga}$	—	8.025
$\text{Sc}_3\text{Al}$	—	8.150

<sup>a</sup>See Ref. 16

between the two series of compounds:  $\text{Sc}_3\text{XB}$  and  $\text{Sc}_3\text{X}$ , the electronic structure calculations for the three hypothetical structures,  $\text{Sc}_3\text{Al}$ ,  $\text{Sc}_3\text{Ga}$ , and  $\text{Sc}_3\text{Tl}$ , were also performed.

In all cubic  $\text{Sc}_3\text{X}$  structures, lattice constants were derived from the total energy calculations, and MT sphere radii for both Sc and X atoms were set to  $0.35a_0$  (other computational details are the same as in Sec. II A). Table VI presents the calculated values of equilibrium lattice parameter  $a_0$ . The variation of  $a_0$  with X-element in  $\text{Sc}_3\text{X}$  is similar to the tendency observed in  $\text{Sc}_3\text{XB}$ . However, there is much larger difference (3%) between the theoretical and experimental values for  $\text{Sc}_3\text{In}$ , but still within the acceptable error of LDA. This prompted us to study electronic structure as a function of lattice constant in this compound.

First we have analyzed the nonpolarized DOS and the Stoner product  $\text{In}(E_F)$  for  $\text{Sc}_3\text{X}$  compounds (Table VII). In view of the KKR results, the Stoner criterion is not fulfilled only in  $\text{Sc}_3\text{Ga}$  and  $\text{Sc}_3\text{Al}$ , and indeed, the spin-polarized KKR computations yielded nonmagnetic ground state in both cases (non-spin-polarized DOS are shown in Fig. 9).

In agreement with the Stoner analysis, spin-polarized KKR computations in  $\text{Sc}_3\text{Tl}$  and  $\text{Sc}_3\text{In}$  converged to ferromagnetic ground state (see Fig. 10) with magnetic moments as large as  $0.37\mu_B$  and  $0.25\mu_B$  per scandium atom for the cases of  $X=\text{Tl}$  and  $\text{In}$ , respectively. The magnetic moment on X atom was negligible ( $\approx 0.02\mu_B$ ). From the calculations for

TABLE VII. Electronic properties of  $\text{Sc}_3\text{X}$ .  $n(E_F)$  is given in 1/Ry per spin per formula unit,  $n_{\text{Sc}}$  in 1/Ry per spin per atom, and  $\mu_{\text{Sc}}$  in  $\mu_B$  per scandium atom.

Non-spin-polarized calculations					
Compound	$n(E_F)$	$n_{\text{Sc}}(E_F)$	$\text{In}(E_F)$		
$\text{Sc}_3\text{Tl}$	91.2	30.1	1.78		
$\text{Sc}_3\text{In}$	62.1	19.9	1.17		
$\text{Sc}_3\text{Ga}$	45.9	14.4	0.89		
$\text{Sc}_3\text{Al}$	37.2	11.8	0.70		
$\text{Sc}_3\text{In (hex)}$	72.8	23.0	1.32		
Spin-polarized calculations					
Compound	$n_{\uparrow}(E_F)$	$n_{\downarrow}(E_F)$	$n_{\uparrow\text{Sc}}(E_F)$	$n_{\downarrow\text{Sc}}(E_F)$	$\mu_{\text{Sc}}$
$\text{Sc}_3\text{Tl}$	43.3	26.4	14.2	8.5	0.37
$\text{Sc}_3\text{In}$	49.6	34.7	15.7	11.0	0.25
$\text{Sc}_3\text{In (hex)}$	69.7	27.5	19.3	8.5	0.32



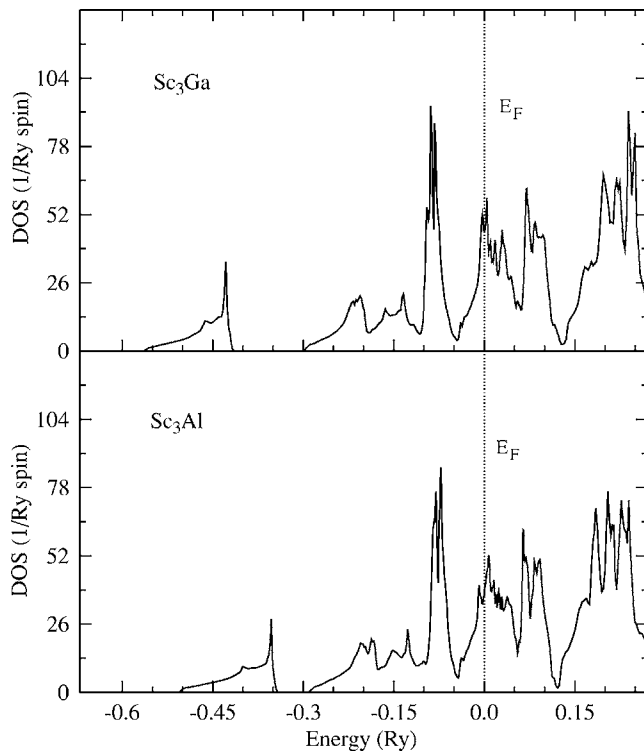


FIG. 9. KKR nonpolarized total DOS in  $\text{Cu}_3\text{Au}$ -type  $\text{Sc}_3\text{Ga}$  and  $\text{Sc}_3\text{Al}$ , calculated at equilibrium lattice constants  $a_0$ . The Fermi level is shifted to zero and marked by a vertical line.

$\text{Sc}_3\text{In}$ , magnetic moments on scandium in the cubic and hexagonal<sup>73</sup> phase are quite similar (see Table VII). The magnetic moment variation with lattice constant for  $\text{Sc}_3\text{X}$  ferromagnets is shown in Fig. 11. The observed monotonic decrease of magnetization with the cell volume shrinking indicates, that magnetization may disappear under hydrostatic pressure. Conversely, magnetization in hexagonal  $\text{Sc}_3\text{In}$  enhances<sup>62</sup> under moderate hydrostatic pressure, which was supported by electronic structure calculations<sup>63</sup> suggesting an increase of magnetic moment under weak hydrostatic pressure, while suppression of ferromagnetism upon applying the uniaxial strain.

It seems interesting to recall, that other widely investigated weak ferromagnet  $\text{Ni}_3\text{Al}$ <sup>64</sup> crystallizes in the same  $\text{Cu}_3\text{Au}$ -type structure. In addition, the electronic structure calculations in  $\text{Ni}_3\text{Al}$  gave a small magnetic moment on Ni ( $\mu_{\text{Ni}} \approx 0.24\mu_B$ ),<sup>65</sup> which is close to the KKR value we have gained for scandium in the cubic  $\text{Sc}_3\text{In}$  ( $\mu_{\text{Sc}} \approx 0.25\mu_B$ ). According to measurements,<sup>64</sup>  $\text{Ni}_3\text{Al}$  exhibits weak itinerant magnetism, however with much smaller magnetic moment  $\mu_{\text{Ni}} = 0.075\mu_B$ . Surprisingly, the similar compound  $\text{Ni}_3\text{Ga}$  was found experimentally to be paramagnetic,<sup>64</sup> although LDA calculations resulted in the magnetic state with  $\mu_{\text{Ni}} = 0.26\mu_B$ ,<sup>65</sup> value even larger than in  $\text{Ni}_3\text{Al}$ . The discrepancy between LDA prediction and experimental finding in  $\text{Ni}_3\text{Ga}$  was explained in terms of strong spin fluctuations.<sup>65</sup>

#### D. Ferromagnetism versus superconductivity

Studying possible competition of superconductivity and weak ferromagnetism is directly related to investigation of

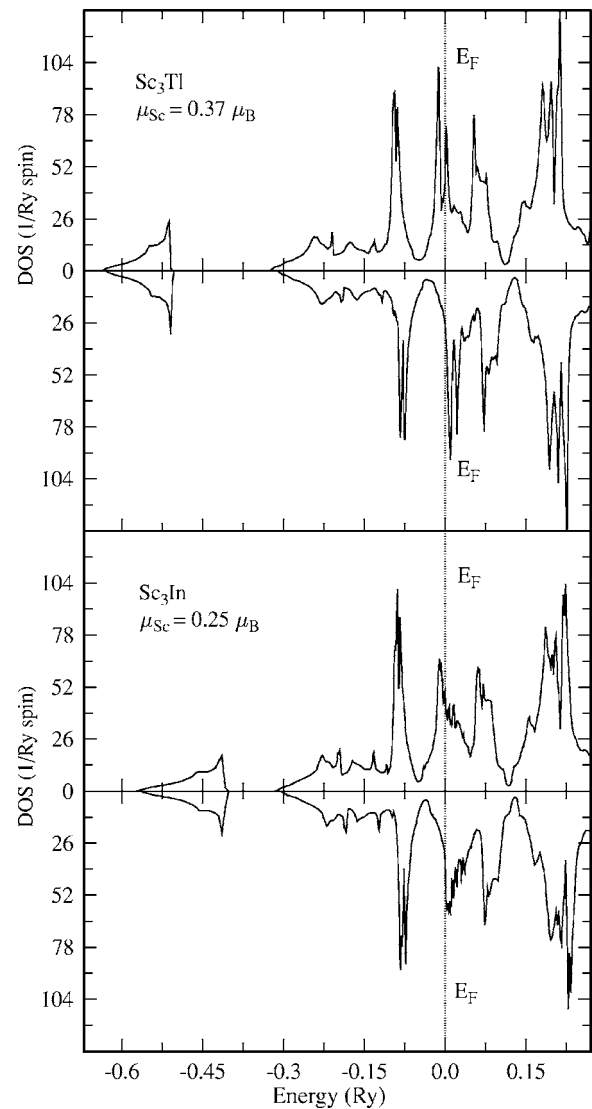


FIG. 10. KKR polarized total DOS in  $\text{Cu}_3\text{Au}$ -type  $\text{Sc}_3\text{Tl}$  and  $\text{Sc}_3\text{In}$ , calculated at equilibrium lattice constant  $a_0$ . The Fermi level is shifted to zero and marked by a vertical line.

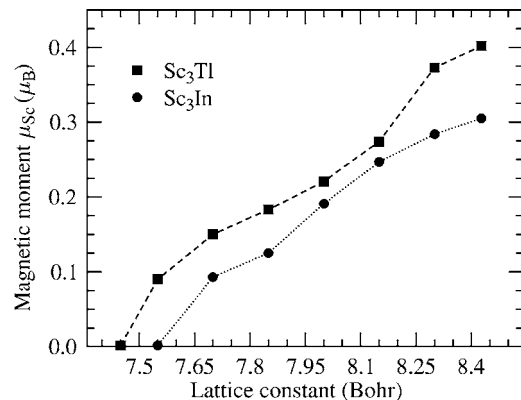


FIG. 11. Magnetic moment on the scandium atom in  $\text{Sc}_3\text{Tl}$  and  $\text{Sc}_3\text{In}$  as a function of the lattice constant. Lines are added as a guide for the eye.

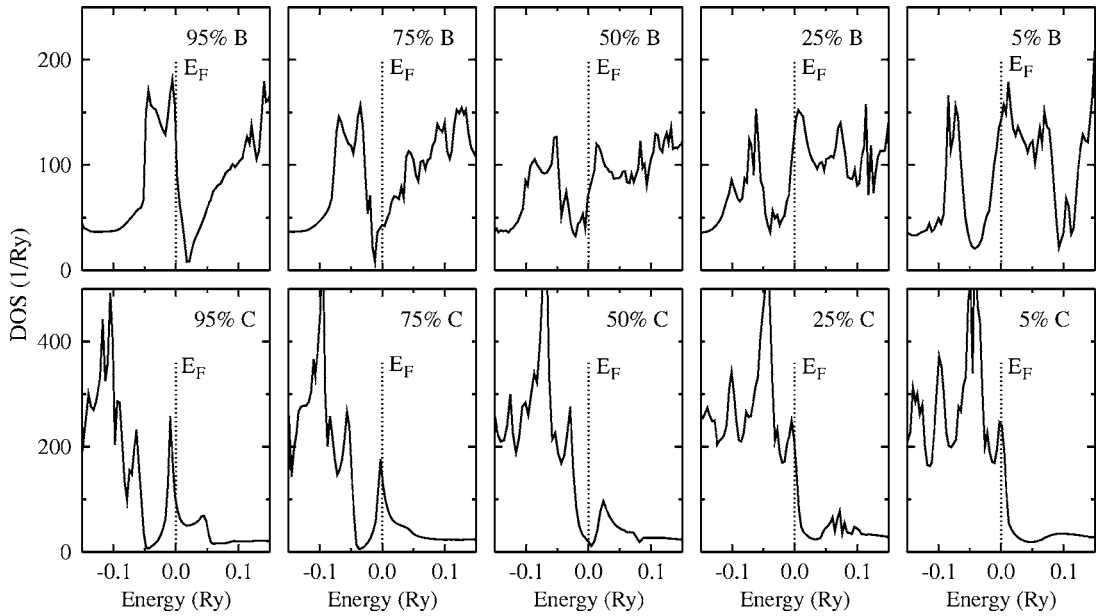


FIG. 12. Effect of vacancy on total density of states in  $\text{Sc}_3\text{InB}_x$  (upper panels) and  $\text{MgC}_x\text{Ni}_3$  (lower panels) from KKR-CPA calculations. Note a remarkable evolution of electronic states in the vicinity of the Fermi level: from high DOS at  $E_F$  in C-rich and B-rich samples (left side: i.e., near full C/B occupancy and superconductivity limit) through a deep DOS minimum (intermediate concentrations; i.e., near 50% C in  $\text{MgC}_x\text{Ni}_3$  and  $\sim 80\%$  B in  $\text{Sc}_3\text{InB}_x$ ) to again large DOS, which satisfy the Stoner criterion (right side: i.e., near empty C/B sublattice limit). The Fermi level is at zero, marked by a vertical line.

the role of trivalent boron in the entitled compounds. To enlighten this subject, the KKR-CPA calculations were performed for illustrative example of  $\text{Sc}_3\text{InB}_x$ , in full range of B concentration.

Analyzing the nonmagnetic DOS values for  $\text{Sc}_3\text{In}$  (see Table VII), one notices that the large  $n(E_F)$  value consists mainly (over 95%) of scandium atoms' contribution. This gives a large Stoner product on Sc and makes the magnetic ground state energetically favorable. The DOS evolution (see Fig. 12) shows that when B concentration increases, the Fermi level shifts from the strongly increasing DOS (5% B in Fig. 12), leaving the “magnetic” region, towards a deep valley (75% B in Fig. 12). After crossing this minimum, the  $n(E_F)$  value again increases, but the Stoner limit on Sc is not reached here (95% B in Fig. 12). The total DOS at  $E_F$ , as well as the scandium contribution  $n_{\text{Sc}}(E_F)$  in  $\text{Sc}_3\text{InB}$ , are much lower than the corresponding values in  $\text{Sc}_3\text{In}$ . Consequently, the Stoner product in  $\text{Sc}_3\text{InB}$  is as small as 0.5, which prevents formation of magnetic ground state.

In order to better understand the mechanism of lowering the scandium contribution to  $n(E_F)$ , we can notice an interesting result concerning the formation of one additional low-lying band in  $\text{Sc}_3\text{InB}$  (two lowest-lying bands below  $-0.3$  Ry in Fig. 3, against only one in  $\text{Sc}_3\text{In}$  in Fig. 13). This band is formed from hybridization of  $s$ -like states from B with Sc orbitals (including  $d$ -states) and presumably bounds about one electron from B and one electron from Sc. Consequently, the energy bands in  $\text{Sc}_3\text{InB}$  in the range of  $-0.3 \text{ Ry} < E < E_F$  include one Sc electron less than the bands in  $\text{Sc}_3\text{In}$  in the corresponding energy range.

When comparing integrated partial  $d$ -DOS for Sc atom in both compounds, we clearly notice the decrease of  $d$ -Sc orbitals filling in  $\text{Sc}_3\text{InB}$ : 1.5 electron versus 1.7 in  $\text{Sc}_3\text{In}$  (per

Sc atom) as well as the transfer of about 0.1 electron from upper bands to the lower, additional band, for each Sc atom.

These two effects show the important modification of valence states of Sc upon B insertion, and seem also to be responsible for lowering the scandium contribution to  $n(E_F)$  and preventing the ferromagnetism. When the ferromagnetic ground state in  $\text{Sc}_3\text{InB}$  (and  $\text{Sc}_3\text{TlB}$ ) is destroyed, the conventional superconductivity is allowed to appear. Certainly, the presence of boron atom is not only important for prevent-

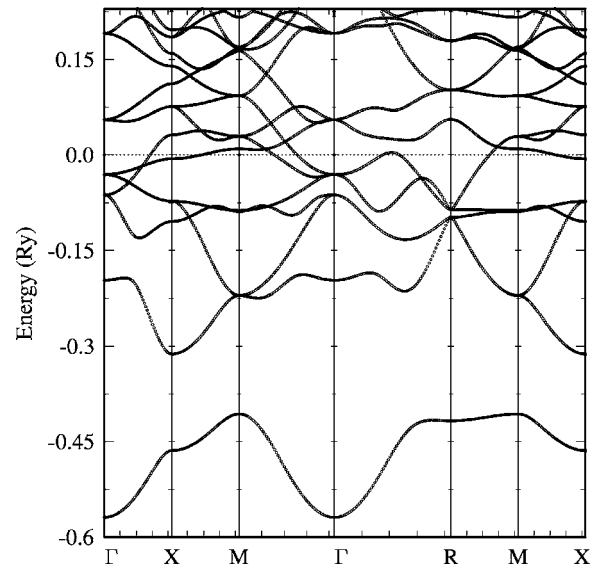


FIG. 13. The nonpolarized electronic dispersion curves  $E(k)$  along high-symmetry directions in cubic  $\text{Sc}_3\text{In}$ , calculated at equilibrium lattice constant  $a_0$ . The Fermi level is marked by a horizontal line.

ing ferromagnetism, but, as we have seen in Sec. II B, it is crucial to promote superconductivity. This opens the perspectives of interesting experimental study, if it were possible to synthesize the  $\text{Sc}_3\text{XB}_x$  systems with various boron concentrations.

Appearance of a magnetic ground state in  $\text{Sc}_3\text{Tl}$  and  $\text{Sc}_3\text{In}$  makes  $\text{Sc}_3\text{TlB}$  and  $\text{Sc}_3\text{InB}$  even more similar to  $\text{MgCNi}_3$ , since the hypothetical  $\text{Cu}_3\text{Au}$ -type structure  $\text{MgNi}_3$  was theoretically predicted to have a small magnetic moment (about  $0.4\mu_B$  per Ni atom<sup>66</sup>). We may confirm this result ( $\mu_{\text{Ni}}=0.40\mu_B$  from KKR).

For comparison with  $\text{Sc}_3\text{InB}_x$ , we present the evolution of the electronic structure for  $\text{MgC}_x\text{Ni}_3$  in Fig. 12. The DOS variation with C concentration is a bit different, since  $E_F$  moves towards lower-lying valence states when the carbon concentration decreases, in contrast to the  $\text{Sc}_3\text{InB}_x$  system. However, the general trends are quite similar in both cases. When C concentration decreases, the Fermi level crosses the DOS valley, and next falls into the higher-DOS region, where a magnetic ground state appears. It is also worth noting that the van Hove singularity near  $E_F$  in  $\text{MgCNi}_3$ , being the unusual feature of its electronic structure, disappears when the vacancy concentration increase (due to the deficiency of carbon  $p$ -orbitals). Note that our DOS picture for  $x=75\%$  compares well with the result obtained for  $x=80\%$  in Ref. 61.

Interestingly, the comparison of data presented in Tables III and VII suggest that the strength of *magnetic* interactions in  $\text{Sc}_3X$  and the *electron-phonon* interactions in  $\text{Sc}_3\text{XB}$  seem to be correlated, since both the Stoner product  $\text{In}(E_F)$  and EPC parameter  $\lambda$  are increasing with  $X$ ; i.e., the lowest values are observed for  $X=\text{Al}$  and highest ones for  $X=\text{Tl}$ .

### III. CONCLUSIONS

We have presented a theoretical investigation of superconducting properties of the perovskite series  $\text{Sc}_3\text{XB}$  ( $X=\text{Tl, In, Ga, Al}$ ) and their possible connections with weak magnetism in the corresponding  $\text{Sc}_3X$  compounds. Summarizing our main results in this paper, we predict:

(i) superconductivity in  $\text{Sc}_3\text{XB}$ , with  $\lambda \approx 0.7-1.25$  and  $T_c \approx 7-15$  K;

(ii) weak ferromagnetism in  $\text{Sc}_3\text{In}$  and  $\text{Sc}_3\text{Tl}$  and the absence of ferromagnetism in  $\text{Sc}_3\text{Ga}$  and  $\text{Sc}_3\text{Al}$ ;

(iii) critical effect of a vacancy on the B site on superconductivity in  $\text{Sc}_3\text{XB}_x$ .

We have also shown, that boron, inserted to the cubic  $\text{Sc}_3\text{Tl}$  and  $\text{Sc}_3\text{In}$ , destroys the magnetic ground state, and likely turns these systems into superconductors.

On the whole, the estimated EPC parameters and critical temperatures  $T_c$ , obtained for  $\text{Sc}_3\text{XB}$  compounds from the RMTA analysis, are even larger than the values reported for two perovskite superconductors  $\text{MgCNi}_3$  and  $\text{YRh}_3\text{B}$ .

A preliminary experimental study of one of the compounds from the entitled series,  $\text{Sc}_3\text{InB}$ , was undertaken.<sup>14</sup> However, several synthesis procedures did not succeed in preparing a single-phase and stoichiometric compound, but one of the samples showed signs of superconductivity with  $T_c \approx 4.5$  K. Further experimental study is needed to clarify this situation.

Moreover, in view of the fact that some itinerant ferromagnets exhibit superconducting properties, e.g.,  $\text{Y}_9\text{Co}_7$  (see Ref. 67) or  $\text{UGe}_2$ ,<sup>68</sup> the experimental investigation of cubic series  $\text{Sc}_3X$  should also be appealing.

\*Corresponding author, electronic mail: tobola@ftj.agh.edu.pl

<sup>1</sup>T. He, Q. Huang, A. P. Ramirez, Y. Wang, K. A. Regan, N. Rogado, M. A. Hayward, M. K. Haas, J. S. Slusky, K. Inumara *et al.*, Nature (London) **411**, 54 (2001)..

<sup>2</sup>H. Rosner, R. Weht, M. D. Johannes, W. E. Pickett, and E. Tosatti, Phys. Rev. Lett. **88**, 027001 (2002).

<sup>3</sup>T. G. Kumary, J. Janaki, A. Mani, S. M. Jaya, V. S. Sastry, Y. Hariharan, T. S. Radhakrishnan, and M. C. Valsakumar, Phys. Rev. B **66**, 064510 (2002).

<sup>4</sup>G. Garbarino, M. Monteverde, M. Nez-Regueiro, C. Acha, R. Weht, T. He, K. A. Regan, N. Rogado, M. Hayward, and R. J. Cava, Physica C **408**, 754 (2004).

<sup>5</sup>Z. Q. Mao, M. M. Rosario, K. D. Nelson, K. Wu, I. G. Deac, P. Schiffer, Y. Liu, T. He, K. A. Regan, and R. J. Cava, Phys. Rev. B **67**, 094502 (2003).

<sup>6</sup>R. Prozorov, A. Snezhko, T. He, and R. J. Cava, Phys. Rev. B **68**, 180502(R) (2003).

<sup>7</sup>J. Y. Lin, P. L. Ho, H. L. Huang, P. H. Lin, Y. L. Zhang, R. C. Yu, C. Q. Jin, and H. D. Yang, Phys. Rev. B **67**, 052501 (2003).

<sup>8</sup>P. M. Singer, T. Imai, T. He, M. A. Hayward, and R. J. Cava, Phys. Rev. Lett. **87**, 257601 (2001).

<sup>9</sup>T. Klimczuk and R. J. Cava, Phys. Rev. B **70**, 212514(R) (2004).

<sup>10</sup>H. Takei, N. Kobayashi, H. Yamauchi, T. Shishido, and T.

Fukase, J. Less-Common Met. **125**, 233 (1986).

<sup>11</sup>R. E. Schaak, M. Avdeev, W.-L. Lee, G. Lawes, H. W. Zandbergen, J. D. Jorgensen, N. P. Ong, A. P. Ramirez, and R. J. Cava, J. Solid State Chem. **177**, 1244 (2004).

<sup>12</sup>M.-S. Park, J. Giim, S.-H. Park, Y. W. Lee, S. I. Lee, and E. J. Choi, Supercond. Sci. Technol. **17**, 274 (2004).

<sup>13</sup>M. D. Johannes and W. E. Pickett, Phys. Rev. B **70**, 060507(R) (2004).

<sup>14</sup>B. Wiendlocha, J. Tobola, S. Kaprzyk, D. Fruchart, and J. Marcus, The European Conference Physics of Magnetism'05, 24-27 June 2005, Poznan, Poland; B. Wiendlocha, J. Tobola, S. Kaprzyk, D. Fruchart, and J. Marcus, Phys. Status Solidi B **243**, 351 (2006).

<sup>15</sup>H. Holleck, J. Less-Common Met. **52**, 167 (1977).

<sup>16</sup>A. Palenzona, P. Manfrinetti, and R. Palenzona, J. Alloys Compd. **15**, 94 (1996).

<sup>17</sup>J. F. Cannon, in Proceedings of the Ninth AIRAPT International High Pressure Conference, 1984, p. 113.

<sup>18</sup>B. T. Matthias, A. M. Clogston, H. J. Williams, E. Corenzwit, and R. C. Sherwood, Phys. Rev. Lett. **7**, 7 (1961).

<sup>19</sup>W. L. McMillan, Phys. Rev. **167**, 331 (1968).

<sup>20</sup>J. J. Hopfield, Phys. Rev. **186**, 443 (1969).

<sup>21</sup>G. D. Gaspari and B. L. Gyorffy, Phys. Rev. Lett. **28**, 801 (1972).

- <sup>22</sup>W. E. Pickett, Phys. Rev. B **25**, 745 (1982).
- <sup>23</sup>I. I. Mazin, S. N. Rashkeev, and S. Y. Savrasov, Phys. Rev. B **42**, 366 (1990).
- <sup>24</sup>A. D. Zdetsis, E. N. Economou, and D. A. Papaconstantopoulos, Phys. Rev. B **24**, 3115 (1981).
- <sup>25</sup>W. H. Butler, J. J. Olson, J. S. Faulkner, and B. L. Gyorffy, Phys. Rev. B **14**, 3823 (1976).
- <sup>26</sup>W. H. Butler, Phys. Rev. B **15**, 5267 (1977).
- <sup>27</sup>S. Y. Savrasov and D. Y. Savrasov, Phys. Rev. B **54**, 16487 (1996).
- <sup>28</sup>D. A. Papaconstantopoulos, L. L. Boyer, B. M. Klein, A. R. Williams, V. L. Morruzzi, and J. F. Janak, Phys. Rev. B **15**, 4221 (1977).
- <sup>29</sup>S. S. Rajput, R. Prasad, R. M. Singru, S. Kaprzyk, and A. Bansil, J. Phys.: Condens. Matter **8**, 2929 (1996).
- <sup>30</sup>B. M. Klein, L. L. Boyer, and D. A. Papaconstantopoulos, Phys. Rev. Lett. **42**, 530 (1979).
- <sup>31</sup>B. M. Klein and D. A. Papaconstantopoulos, Phys. Rev. Lett. **32**, 1193 (1974).
- <sup>32</sup>S. V. Halilov, D. J. Singh, and D. A. Papaconstantopoulos, Phys. Rev. B **65**, 174519 (2002).
- <sup>33</sup>W. E. Pickett and D. J. Singh, Phys. Rev. Lett. **72**, 3702 (1994).
- <sup>34</sup>D. A. Papaconstantopoulos and B. M. Klein, Phys. Rev. Lett. **35**, 110 (1975).
- <sup>35</sup>J. Kortus, I. I. Mazin, K. D. Belashchenko, V. P. Antropov, and L. L. Boyer, Phys. Rev. Lett. **86**, 4656 (2001).
- <sup>36</sup>W. E. Pickett, Rev. Mod. Phys. **61**, 433 (1989).
- <sup>37</sup>H. J. Choi, D. Roundy, H. Sun, M. L. Cohen, and S. G. Louie, Nature (London) **418**, 758 (2002).
- <sup>38</sup>A. Floris, G. Profeta, N. N. Lathiotakis, M. Luders, M. A. L. Marques, C. Franchini, E. K. U. Gross, A. Continenza, and S. Massidda, Phys. Rev. Lett. **94**, 037004 (2005).
- <sup>39</sup>A. Bansil, S. Kaprzyk, P. E. Mijnen, and J. Tobola, Phys. Rev. B **60**, 13396 (1999).
- <sup>40</sup>*Applications of Multiple Scattering Theory to Materials Science*, edited by W. H. Butler, P. Dederichs, A. Gonis, and R. Weaver, MRS Symposia Proceedings No. 253 Materials Research Society, Pittsburgh, 1992, Chap. III.
- <sup>41</sup>S. Bei der Kellen, Y. Oh, E. Badraxe, and A. J. Freeman, Phys. Rev. B **51**, 9560 (1995).
- <sup>42</sup>M. Ogura and H. Akai, J. Phys.: Condens. Matter **17**, 5741 (2005).
- <sup>43</sup>T. Stopa, S. Kaprzyk, and J. Tobola, J. Phys.: Condens. Matter **16**, 4921 (2004).
- <sup>44</sup>J. P. Perdew and Y. Wang, Phys. Rev. B **45**, 13244 (1992).
- <sup>45</sup>S. Baroni, A. Dal Corso, S. de Gironcoli, and P. Giannozzi, www.pwscf.org
- <sup>46</sup>S. Baroni, A. Dal Corso, S. de Gironcoli, and P. Giannozzi, Rev. Mod. Phys. **73**, 515 (2001).
- <sup>47</sup>J. P. Perdew and A. Zunger, Phys. Rev. B **23**, 5048 (1981).
- <sup>48</sup>M. Methfessel and A. T. Paxton, Phys. Rev. B **40**, 3616 (1989).
- <sup>49</sup>P. B. Allen and R. C. Dynes, Phys. Rev. B **12**, 905 (1975).
- <sup>50</sup>G. Grimvall, *The Electron-Phonon Interaction in Metals* (North-Holland, Amsterdam, 1981).
- <sup>51</sup>P. Ravindran, S. Sankaralingam, and R. Asokamani, Phys. Rev. B **52**, 12921 (1995).
- <sup>52</sup>P. J. T. Joseph and P. P. Singh, cond-mat/0505310 v1 (unpublished).
- <sup>53</sup>S. B. Dugdale and T. Jarlborg, Phys. Rev. B **64**, 100508(R) (2001).
- <sup>54</sup>A. Szajek, J. Phys.: Condens. Matter **13**, 595 (2001).
- <sup>55</sup>R. Heid, B. Renker, H. Schober, P. Adelman, D. Ernst, and K. P. Bohnen, Phys. Rev. B **69**, 092511 (2004).
- <sup>56</sup>A. Y. Ignatov, S. Y. Savrasov, and T. A. Tyson, Phys. Rev. B **68**, 220504(R) (2003).
- <sup>57</sup>A. Y. Ignatov, L. M. Dieng, T. A. Tyson, T. He, and R. J. Cava, Phys. Rev. B **67**, 064509 (2003).
- <sup>58</sup>T. Amos, Q. Huang, J. Lynn, T. He, and R. Cava, Solid State Commun. **121**, 73 (2002).
- <sup>59</sup>Z. A. Ren, G. C. Che, S. L. Jia, H. Chen, Y. M. Ni, G. D. Liu, and Z. X. Zhao, Physica C **371**, 1 (2002).
- <sup>60</sup>A. Walte, G. Fuchs, K.-H. Muller, S.-L. Drechsler, K. Nenkov, and L. Schultz, Phys. Rev. B **72**, 100503(R) (2005).
- <sup>61</sup>P. J. Joseph and P. P. Singh, Phys. Rev. B **72**, 064519 (2005).
- <sup>62</sup>J. Grewe, J. S. Schilling, K. Ikeda, and K. A. Gschneidner, Jr., Phys. Rev. B **40**, 9017 (1989).
- <sup>63</sup>A. Aguayo and D. J. Singh, Phys. Rev. B **66**, 020401(R) (2002).
- <sup>64</sup>F. R. de Boer, C. J. Schinkel, J. Biesterbos, and S. Proost, J. Appl. Phys. **40**, 1049 (1969).
- <sup>65</sup>A. Aguayo, I. I. Mazin, and D. J. Singh, Phys. Rev. Lett. **92**, 147201 (2004).
- <sup>66</sup>J. H. Shim, S. K. Kwon, and B. I. Min, Phys. Rev. B **64**, 180510(R) (2001).
- <sup>67</sup>A. Kolodziejczyk and J. Spalek, J. Phys. F: Met. Phys. **14**, 1277 (1984).
- <sup>68</sup>S. S. Saxena, P. Agarwal, K. Ahilan, F. M. Grosche, R. K. W. Hasselwimmer, M. J. Steiner, E. Pugh, I. R. Walker, S. R. Julian, P. Monthoux *et al.*, Nature (London) **406**, 587 (2000).
- <sup>69</sup>V. B. Compton and B. T. Matthias, Acta Crystallogr. **15**, 94 (1962).
- <sup>70</sup>For a review of the MgCNi<sub>3</sub> properties see also the recent papers on this subject, e.g., Refs. 9 and 61.
- <sup>71</sup>Definition of the *n*th frequency moment of the Eliashberg coupling function  $\alpha^2F(\omega)$ :<sup>49,50</sup>  $\langle\omega^n\rangle = \int \omega^{n-1} \alpha^2F(\omega) d\omega / \int \omega^{-1} \alpha^2F(\omega) d\omega$ . If  $\alpha^2(\omega) \approx \text{const}$ ,  $\langle\omega^n\rangle \approx \int \omega^{n-1} F(\omega) d\omega / \int \omega^{-1} F(\omega) d\omega$ .  $\alpha^2(\omega)$  is the electron-phonon interaction coefficient.
- <sup>72</sup>The values of  $n(E_F)$  presented in Table II for Sc<sub>3</sub>InB are a bit different from those in Ref. 14. It comes from an applied smaller lattice parameter (the equilibrium value instead of the experimental one) and semirelativistic effects, present in this work. Because the Fermi level is located on the slope of DOS peak, small shift in  $E_F$  has a noticeable influence on  $n(E_F)$ . However,  $\eta$  values are not affected much, because they are defined as a ratio of resulting densities.
- <sup>73</sup>In the Ni<sub>3</sub>Sn-type Sc<sub>3</sub>In experimental lattice constants were taken:  $a=6.42 \text{ \AA}$ ,  $c=5.18 \text{ \AA}$ ,<sup>69</sup> the adjustable parameter  $x$ , positioning Sc atoms in the XY plane, was assumed to have the ideal value of  $x=5/6$ , following x-ray analysis<sup>69</sup> and previous calculations.<sup>63</sup> The same MT sphere radius (3.0 Bohr) was used for Sc and In. In the present work, the magnetic moment is given per Wigner-Seitz cell and per Sc atom. In Ref. 14, the magnetic moments of  $0.26 \mu_B$  (hexagonal phase) and  $0.27 \mu_B$  (cubic phase, experimental lattice constant), were given per Sc MT sphere.